Supplementary Data on Fiber misalignment analysis in PCM-UD composite materials by Full Field Nodal Method

S1. Algorithm for corner's detection

In a first step, each of the 3 channels of the original RGB image (Figure S 1 a) was equalized, and a median filter was applied to mitigate the noise. Images showed several drops resp agglomeration of release agent residues [1]: their high repeatability in color allowed to implement of a custom RGB filter to remove them; results are shown in Figure S 1 b.

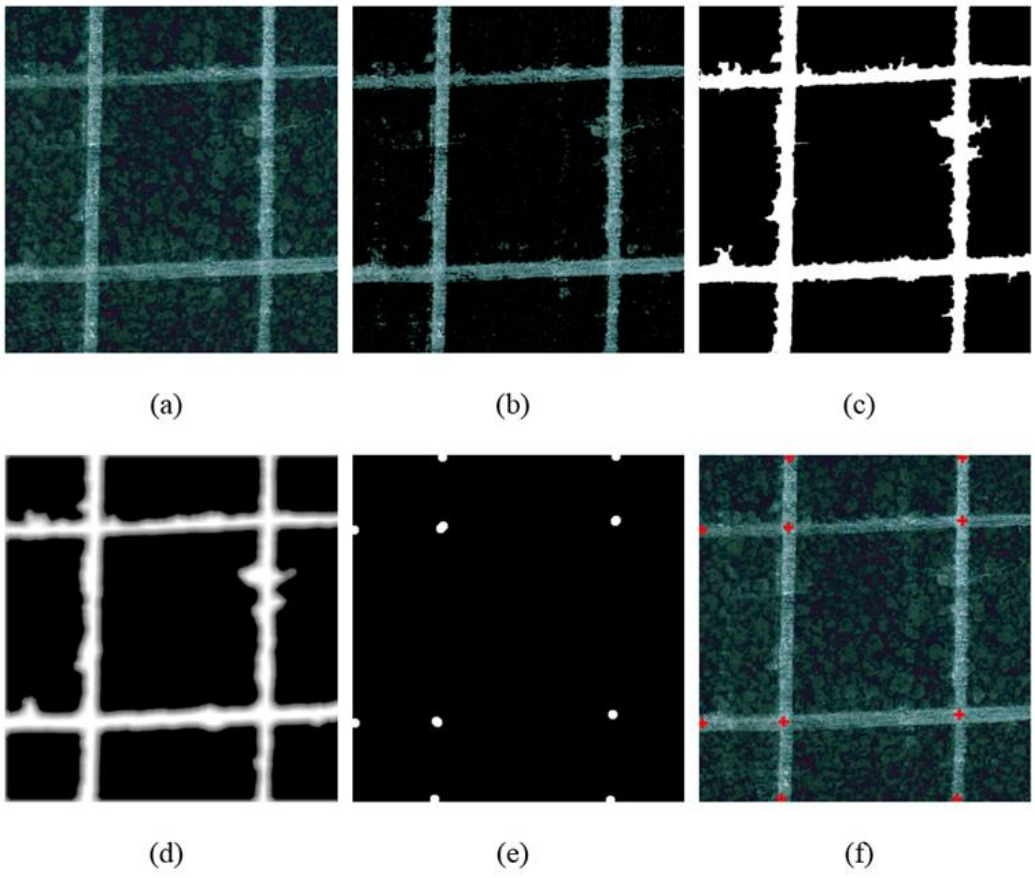

Figure S 1: Step-by-step image processing on a portion of the plate. a) original image b) image after RGB filtering c) image after binarization d) average filtered BW image e) dilatated branch point of the BW image f) original image with corners detected by the algorithm.

Images were binarized (Figure S 1 c) and eroded employing the "thinning" technique to detect the centerline of the grid: an average filter of 50 pixels was applied on the binary image (Figure

S 1 d) and the 'thin' option of "bwmorph" (an inbuilt Matlab function) [2] was automatically repeated until one-pixel width skeleton was obtained. Spur branches and single unconnected pixels were removed, and branch points of the skeleton were detected by using the 'brenchpoint' option of bwmorph. The grid's corners were finally detected by the coordinates of the centers of mass, shown in Figure S 1 f, of the dilatated branchpoint image (Figure S 1 e).

S2. Prepreg characterization

To account for the initial misalignment, a prepreg characterization was conducted with a similar procedure to the one described in [3]. Six single-ply samples were extracted at different locations from the same roll of prepreg used in section 2.2.1 of the present work. The dimension of the samples was about 100 mm in the 1-direction and 30 mm in the 2-direction. The mid wide of the samples was coincident with the mid wide of the roll and with two lines, located 30 mm far from the edges. To minimize fiber distortions, samples were cured using the vacuum bagging technique in an oven at a temperature of 140°C for 3 hours over a flat aluminum tool with a PTFE layer at the interface. A vacuum of about 101kPa was applied and maintained during the whole curing cycle. After curing, each sample was cut at about 5° in the 1-3 plane and split into 4 wedges as shown in Figure S 2.

Figure S 2: Cured specimen sectioned at 5°

Each wedge was mounted in a cold embedding acrylic resin (Technovit® 4006, Kulzer GmbH, Wehrheim, Germany). Mounted samples were polished using modified metallographic techniques and examined using a Zeiss Axio Observer 3 at a magnification of 200x. Digital

micrograph images were stitched together to cover a larger representative area and analyzed using a custom code written in Matlab R2019a.

The semi-automatic script performs several image modification and ellipse fitting techniques to calculate and output statistics on the population of identified fiber footprints. A frequency table was generated by populating 0.025° wide bins for each analysis.

Due to the high magnification required by the method and the limited depth of field, the focus was frequently fine-adjusted. This fact caused faults in automating image-stitching, and analysis of the specimens' full length was unfeasible. For these reasons, frequency tables on the most extensive possible stitched images were created, bins summed, and finally normalized using the total number of measured fibers for each specimen.

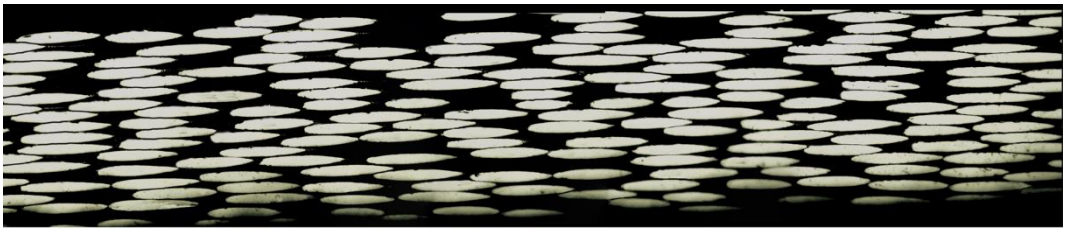

(a)

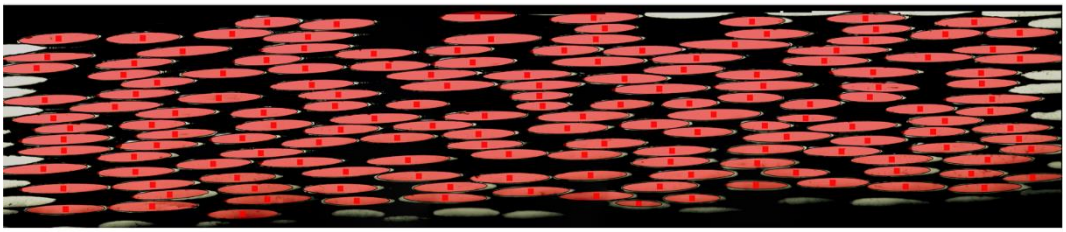

(b)

Figure S 3: Image processing analysis for calculation of fiber orientation. a) stitched image micrograph, b) processed image with ellipse fitting algorithm

The output of the ellipse fitting software is shown in Figure S 3. Concerning Figure S 3 b, the presence of "tails", i.e. sharp corners in white out of the best fitting ellipse, can be identified. However, as demonstrated by Potter and al. [4], they are documented to overestimate the ellipse's major diameter, altering the measurement of in-plane misalignment. For this reason, the code was studied to omit them in processing and calculations.

Results of prepreg characterization are reported in Table S 1. Populations of the 6 samples were always consistent independently from the position on the roll, and a small standard deviation in the range 0.82°-0.92° was observed, thus demonstrating the high alignment in direction 1 of the material used in this study.

Table S 1: In-plane fiber misalignment standard deviation for the material

ID	Axial position	Population	Standard deviation of in-plane misalignments
S1	Left	11287 fibers	0.92°
S2	Center	11094 fibers	0.82°
S3	Right	10974 fibers	0.89°
S4	Left	11107 fibers	0.87°
S5	Center	10473 fibers	0.85°
S6	Right	10893 fibers	0.90°

Indeed, about three-quarters of the literature citing Yourgartis has interpreted the standard deviation as a characteristic angle of the prepreg, sometimes referred to as "initial fiber misalignment" [5–7]. According to its definition, the material's initial fiber misalignment angle is representative of populations of footprints and therefore needs to be treated statistically. The prepreg's overall standard deviation, calculated as "pooled standard deviation" [8] of samples S1-S6, is 0.88° and used by authors to account for the initial misalignment angle prepreg.

[1] Blass D, Dilger K. CFRP-Part Quality as the Result of Release Agent Application - Demoldability, Contamination Level, Bondability. Procedia CIRP, 2017. https://doi.org/10.1016/j.procir.2017.03.219.

[2] Lam L, Lee SW. Thinning methodologies—a comprehensive survey. IEEE Trans Pattern Anal Mach Intell 1992. https://doi.org/10.1109/34.161346.

[3] Stewart AL, Poursartip A. Characterization of fibre alignment in as-received aerospace grade unidirectional prepreg. Compos Part A Appl Sci Manuf 2018. https://doi.org/10.1016/j.compositesa.2018.04.018.

[4] Potter K, Langer C, Hodgkiss B, Lamb S. Sources of variability in uncured aerospace grade unidirectional carbon fibre epoxy preimpregnate. Compos Part A Appl Sci Manuf 2007. https://doi.org/10.1016/j.compositesa.2006.07.010.

[5] Varandas LF, Catalanotti G, Melro AR, Tavares RP, Falzon BG. Micromechanical modelling of the longitudinal compressive and tensile failure of unidirectional composites: The effect of fibre misalignment introduced via a stochastic process. Int J Solids Struct 2020. https://doi.org/10.1016/j.ijsolstr.2020.07.022.

[6] Jelf PM, Fleck NA. Compression Failure Mechanisms in Unidirectional Composites. J Compos Mater 1992. https://doi.org/10.1177/002199839202601804.

[7] Tran T, Comas-Cardona S, Abriak NE, Binetruy C. Unified microporomechanical approach for mechanical behavior and permeability of misaligned unidirectional fiber reinforcement. Compos Sci Technol 2010. https://doi.org/10.1016/j.compscitech.2010.04.023.

[8] McNaught AD, Wilkinson A. IUPAC. Compendium of Chemical Terminology, 2nd ed. (the "Gold Book"). 1997. https://doi.org/10.1351/goldbook.